Target properties – Plasma dynamics relationship in laser ablation of metals: Common trends for fs, ps and ns irradiation regimes

Stefan Andrei Irimiciuc, Petru-Edward Nica, Maricel Agop, Cristian Focsa

Target properties – plasma dynamics relationship in laser ablation of metals: common trends for fs, ps and ns irradiation regimes

Stefan Andrei Irimiciuc[1,*], Petru-Edward Nica[2], Maricel Agop[2] and Cristian Focsa[3]

[1]National Institute for Lasers, Plasma and Radiation Physics, 077125 Bucharest, Romania

[2] Department of Physics, Gh. Asachi Technical University, 700050 Iasi, Romania

[3]Univ. Lille, CNRS, UMR 8523 - PhLAM - Physique des Lasers Atomes et Molécules, F-59000 Lille, France

***contact :** stefan.irimiciuc@inflpr.ro**;**

Address: National Institute for Laser, Plasma and Radiation Physics, Atomistilor Street, No. 409, Magurele city, Ilfov county, PO :077125, Romania

Abstract

Better understanding of complex relationships between laser-produced plasma dynamics and ablation target material properties is key for optimization of numerous technological and analytical applications. Continuing a previous work [Irimiciuc et al., Appl. Surf. Sci. 417 (2017) 108-118] which proposed empirical laws for some of these relationships (in femtosecond irradiation regime), we present here a systematic study on several metallic targets (Al, Cu, Mn, Ni, Ti, Zn) irradiated by nanosecond, picosecond and femtosecond laser pulses. The experimental approach is based on complementary diagnostics, with the implementation of both electrical and optical techniques for transient plasma characterization. The empirical equations previously reported for femtosecond ablation pulses are now extended to the picosecond and nanosecond regimes.

Keywords: laser ablation, transient plasma diagnostics, optical emission spectroscopy, Langmuir probe.

1. Introduction

Fundamental understanding of the transient plasmas generated by laser ablation is of paramount importance for a number of analytical and technological applications, such as Pulsed Laser Deposition (PLD) of thin films [1,2], micro-machining [3], nano-material synthesis [4] or other analytical applications of laser ablation (Laser Induced Breakdown Spectroscopy (LIBS), laser ablation laser induced fluorescence (LA-LIF), laser ablation laser absorption spectroscopy (LA-LAS), laser ablation inductively coupled plasma mass spectrometry (LA-ICP-MS) or laser ablation inductively coupled plasma optical emission spectroscopy (LA-ICP-OES)) [5]. All these processes involve interaction of matter with pulsed laser radiation in various temporal regimes (i.e. pulse durations), from nanosecond (short) to picosecond to femtosecond (ultra-short). Numerous experimental and theoretical studies have tried to isolate and explain the various (often intricated) phenomena occurring in this interaction, in a sustained effort to solve the complex *target-beam-plasma* relationship for further optimization and control of the applications. From the *beam* pulse duration side, the difficulty in reaching a unified description resides in the fundamentally different mechanisms occurring on the various time scales: if in the ultra-short (fs) regime there are mainly non-thermal phenomena leading to Coulomb explosion as main ejection mechanism [6], in the ns

irradiation regime the thermal mechanisms are dominant at the target level and subsequent ejected plume – laser beam interaction can lead to significant plasma heating. An interesting, worth to study regime is the intermediate ps one, where the pulse duration is on the same timescale as the (heated) electrons – lattice equilibration. When considering the *target* side, the difficulty arises from the wide variety of physical (mechanical, thermal, electrical) properties involved, which occurs from simple, mono-elemental targets to highly-complex composition ones. Finally, the comprehensive study of the laser ablation *plasma* is often made difficult by its transient character, requiring space- and time-resolved sensitive techniques to measure a multitude of parameters, such as (among others) chemical composition (atoms, molecules, clusters, nanoparticles), electrical composition (ionization stages, electron number density), individual species dynamics and energetics, plasma potential etc. Various diagnostic methods are available for this, mainly divided in two categories: optical (fast camera photography [7], interferometry [8], shadowgraphy [9], optical emission spectroscopy [10], laser induced fluorescence [11], Thomson scattering [12] etc.) and electrical (mass spectrometry [13], electrostatic analyzers [14], Langmuir probes [15], Faraday cups [16]). Each of these techniques has intrinsic limitations (for instance, interferometry or Thomson scattering require significantly higher electron densities than the Langmuir probe) and usually reveals only a facet of the plasma dynamics (optical methods usually deal with excited states, while electrical probes provide information only on the charged particles), in a restrained space-time domain. A combined use of (several) techniques from both categories is therefore suitable for a more complete description of the plume evolution.

From an applicative point of view, the systematic (and time-consuming) investigation of the ablation plasma plume is often overlooked. In the PLD technique, the optimization of the grown thin film properties is frequently based on an empirical (trial and error) approach (which is also time- and resource-consuming) and on target-specific strategies. Some studies have nevertheless tried to relate the properties of the deposited film with those of the ablation plasma [17], in an effort to understand and overcome undesirable effects like, e.g., non-congruent transfer [18,19]. More peculiar phenomena such as plume splitting, oscillations, or rebound at the substrate [20,21] may also affect the deposition process and therefore deserve further investigation. A unitary understanding of the *target-beam-plasma-film* interaction would provide a useful tool for the design of optimized PLD processes. However, the intrinsic complexity and interconnectivity of these relationships usually lead to a sequential tackling of each step. Several groups have previously reported on the target-plasma relationship [22–26], focusing on particular aspects of the ablation process like ablation threshold, ablation yield or particle density generated by (common) ns ablation, while other groups focused on laser-produced plasma formation and dynamics in various ablation regimes [27,28], with parallel investigations of the impact on the synthesized thin films [29,30]. Finding general relationships that transcend the ablation regime (ns, ps, fs) or the type of ablated material thus appears as an appealing route to propose and implement universal optimization strategies for the PLD process or other technological/analytical applications.

Continuing ongoing experimental [31-33] and theoretical [34] efforts in the quest for identifying such general trends, we propose here a systematic study on the ablation of several

metals in ns, ps and fs regimes. In a previous paper [31] we evidenced some links between the target physical properties and the generated plasma parameters for fs laser ablation, and proposed for the first time empirical relationships between them. In the current paper, we extend this study to the ps and ns regimes and demonstrate the universality of these relationships, regardless of the ablation laser pulse duration. Optical (fast ICCD camera imaging and space- and time-resolved optical emission spectroscopy - OES) and electrical (Langmuir probe) investigations have been used to link target properties (atomic mass, electrical conductivity) to plasma parameters such as expansion velocity, plasma potential, ion density, electron temperature throughout the plasma plume volume.

2. Experimental set-up

The combined optical-electrical diagnostic set-up was presented in previous papers [20,25,28], thus only a brief overview will be given here. For the present study, 20-mm diameter and 1-mm thickness disks of metals with different physical properties (Al, Cu, Mn, Ni, Ti, Zn) were placed on a rotating target system, inside a stainless-steel vacuum chamber evacuated at 10^{-5} Torr base pressure. The targets were successively irradiated at quasi-normal incidence (AOI < 5°) by femtosecond/picosecond mode-locked Ti:Sa (Spectra Physics Spitfire regenerative amplifier, Tsunami oscillator, 800 nm wavelength, 100 Hz repetition rate, 40 fs and 1 ps pulse durations) and Q-switched Nd:YAG (Quantel Brilliant Eazy, 532 nm, 10 Hz, 10 ns). The energy per pulse for each of the laser systems was as follows : 1.6 mJ for fs, 1.2 mJ for ps and 20 mJ for ns, with each laser beam focused at different spot diameters on the metallic targets (140 μm for fs, 120 μm for ps and 500 μm for ns) to result into similar fluences of ≈10 J/cm^2..

For the optical analysis, the dynamics of the laser-produced plasma (LPP) has been studied by means of a high-resolution monochromator (Acton SP2500i, 500 mm focal length) and an intensified charge-coupled device (ICCD) camera (Roper Scientific PI MAX2-1003-UNIGEN2, 1024×1024 pixels, minimum gating time 2 ns). For fast photography measurements, ICCD sequential pictures of the spectrally unresolved plasma optical emission were recorded at various delays (between 25 ns and 12-20 μs) with respect to the laser pulse. The ICCD camera gate was triggered by a fast response photodiode placed outside the chamber and an internal routine was used to increment the delay between the laser pulse and the gate opening. For spectrally resolved studies, plasma emission from 300μm-wide plume slices (parallel to the target surface) was imaged using a two-lens system (1/10 magnification) onto the entrance slit (30 μm width) of the monochromator. High-resolution spectra were recorded with a 2400 l/mm grating and a slit width of 30 μm, resulting in a spectral resolution of ≈0.02 nm on ≈ 8 nm broad spectrum for a given grating position.

The plasma evolution was also monitored by a cylindrical Langmuir probe [31-33] made of stainless steel (0.8 mm diameter, 5 mm length), placed on the plume expansion axis at various distances from the target (12 measurement points between 5 mm and 40 mm). A detailed view of the experimental arrangement can be found in Fig. 1 of Ref. [20]. The probe was biased at 40 different voltages spanning between -35 V and +35 V using a stabilized DC power source, while the target and vacuum chamber were electrically grounded. The electronic and ionic currents were

measured from the voltage drop on a 4.6 kΩ resistor and the transitory signals were recorded with a digital 600 MHz, 2.5 GS/s Oscilloscope (LeCroy Wave Runner 6200A) at 1 MΩ or 50 Ω input impedance. Each experimental point was recorded by averaging the current signals over 50 laser pulses. The continuous rotation movement of the target offered fresh ablation surfaces per each pulse.

3. Results and discussion

3.1 Plasma global structure by ICCD fast photography

Figure 1 displays as a typical example, the characteristic snapshots of optical emission from plasmas produced in nanosecond, picosecond and femtosecond regimes by ablation of the Ti target. The splitting of the plasma plume in two structures (fast and slow) has been observed as a general feature, for all studied targets and for all three ablation regimes, confirming previous studies (see [20] for a review), where the origin of the first (fast) structure was preferentially assigned to electrical-driven mechanisms, while the second one to subsequent thermally-driven processes. As expected, we observed (for all investigated targets) that the ns-LPP has a stronger global emission intensity and it is described by a larger volume, while the picosecond and femtosecond laser-produced plasmas are more directional and the emission is centered around the expansion axis with reduced lateral extension. Similar results were reported in [35,36], with differences in the width of the ionic distribution of about 30° between the plasma plumes produced by nanosecond and femtosecond ablation. The extended emission of the ns-LPP compared to fs and ps ones is generally accepted as coming from the plasma heating by the "tail" of the laser pulse in the short ablation regime. An interesting observation is that the moment of the plasma split in two structures differs between ns irradiation, where it can be observed after ~150 ns from the laser pulse, and ps and fs regimes, where it is seen after ~50 ns delay. In our opinion, this cannot be fully explained by the plasma heating in ns regime and the difference in kinetic energies of the ejecta (see below) and therefore deserves further investigation.

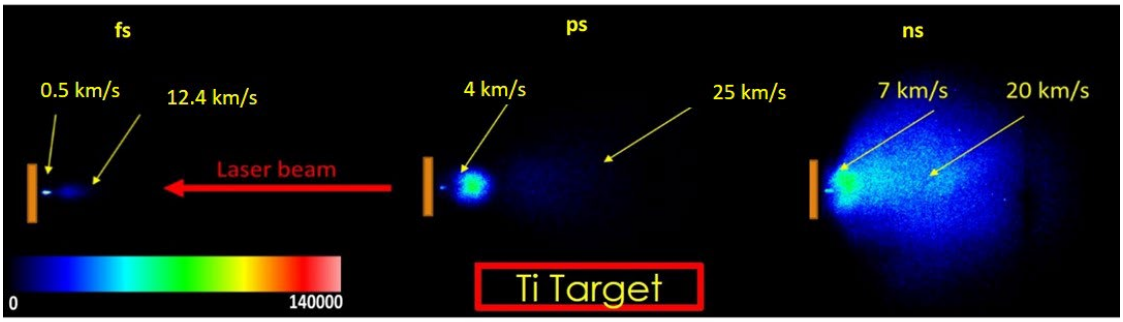

Figure 1. Emission of Ti LPP in fs, ps and ns ablation regimes (ICCD snapshots recorded with 10 ns gate width at 150 ns delay from the laser pulse).

For each ablation regime, the "center-of-mass" expansion velocities [37] of the two structures were estimated by plotting the axial displacement of the maximum emission spots as a function of the delay from the laser pulse. The derived values presented in Figure 2a with respect to the atomic mass of the target material exhibit a decreasing trend as the ejected particles get

heavier (see also [17-19,21]). Among the three irradiation regimes, the ns-LPPs display the highest velocities, ranging from 46.8 km/s for the fast structure and 12.6 km/s for the slow structure in the case of Al target to 18 km/s for the fast structure and 5.5 km/s for the slow one in the case of Zn target. The expansion axial velocities are lower in ps (ranging between 26.8 km/s and 15.1 km/s for the fast structure and between 10 km/s and 4.6 km/s for the slow one) and fs (fast structure: 15.8 – 9.78 km/s and slow structure 3.6 – 0.39 km/s) regimes. Some attempts to explain the relationship between axial expansion velocity (v) and target atomic mass (A) found in the literature [38,39] are mostly based on the classical kinetic energy approach, leading to a $v \propto A^{-1/2}$ dependence. However, by considering such a relation we admit that the particle ejection is driven mainly by thermal mechanisms. This assumption, understandable in the ns ablation regime, does not remain valid in the case of fs or ps regime, where thermal effects are reduced. Therefore, the contribution of other non-thermal mechanisms to the overall values of the plasma plume velocity components should be also considered.

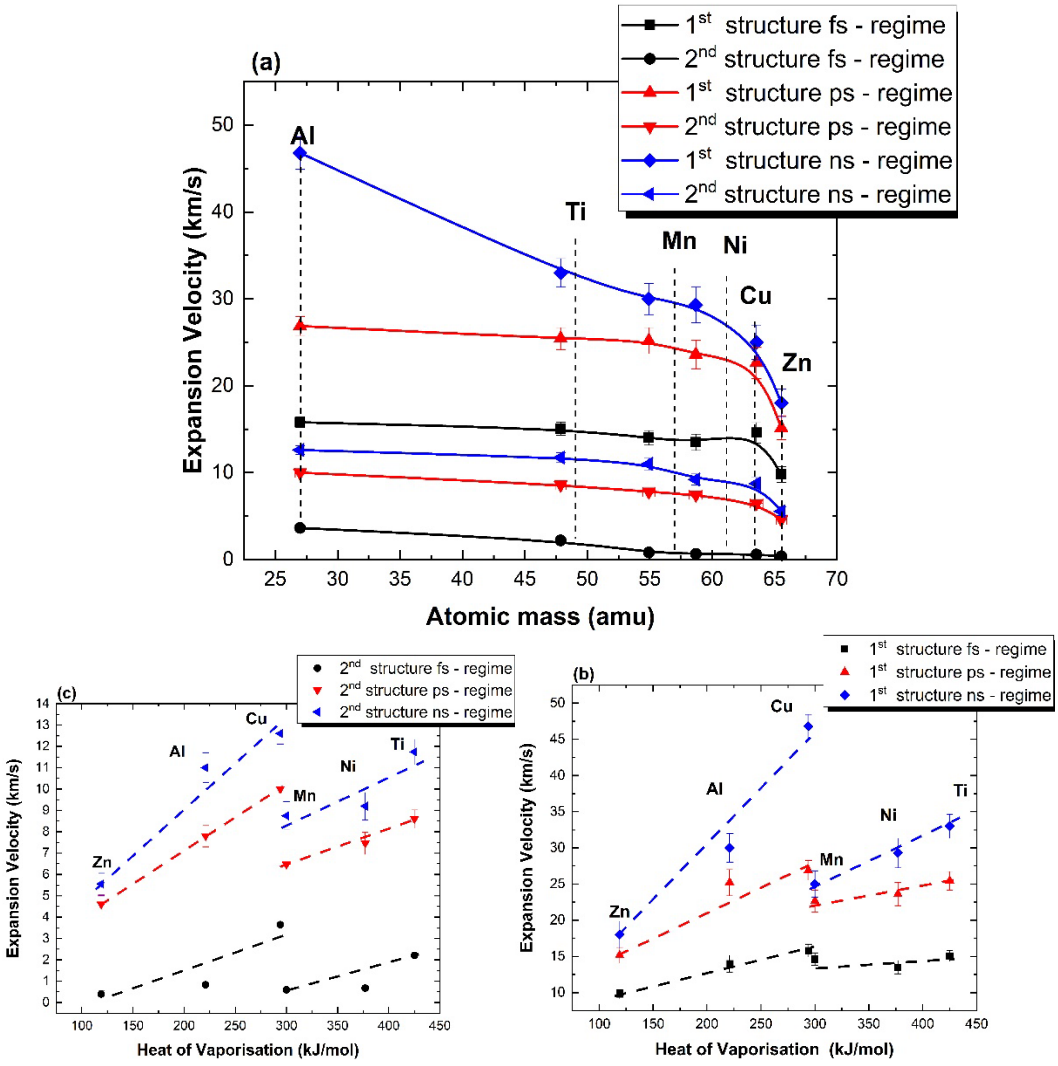

Figure 2. The evolution of the "center-of-mass" expansion velocities of the two plasma structures with the target atomic mass (a) and vaporization heat (b, c) in the three ablation regimes (ns, ps, fs).

When plotting the fast and slow expansion velocities with respect to the vaporization heat of the target material (Figure 2 b,c), we observe that they follow quasi-proportional trends on two distinct regions (< 300 kJ/mol and > 300 kJ/mol) defined by different slopes. The first region includes the Zn, Mn and Al plasmas, while the second one covers the other investigated targets Cu, Ni and Ti. The nature of these quasi-linear evolutions is rather peculiar, as one would rather expect a decrease of the expansion velocity with the heat of vaporization (in the frame of thermal-driven mechanisms [38-42]). Our data suggest that the kinetics of the LPP is not (predominantly) influenced by thermal ejection mechanisms, but rather by electrostatic ones, with an important role of the double layer generated by space charge separation [20,43,44]. Therefore, other physical parameters of the target should be considered (especially for the ps and fs cases where the thermal mechanisms are not as prominent as for the ns case) in order to find the most relevant plasma - target relationships.

3.2 Individual plasma species probed by optical emission spectroscopy

A more "individualized" view (i.e. for individual species in the plasma) of the plume dynamics can be provided by OES, which allows us a qualitative estimation of the contribution of the radiative processes to the total energetic balance. For all investigated plasmas we recorded emission from excited states corresponding to neutral atoms and singly- and doubly-charged ions. The ns-LPP emission lines were more intense compared with the ones generated in fs or ps regimes, as expected due to the plasma heating by the ns pulse [17,21,35].

The excitation temperatures (T_{ex}) of individual plasma species can be easily determined by using the Boltzmann plot method, following for example the procedure described in [27,28,37]. For the present calculations only neutral emission was taking into account, having in view its abundance comparing to those of the singly or multiply charged ions. More than 100 emission lines were used to derive the excitation temperatures from Boltzmann plots. The full list of these lines is available from the corresponding author on request. The resulting excitation temperatures (Figure 3a) exhibit a decrease with the target atomic mass, similar (but more marked) to the one found for the expansion velocities (Figure 2a). The only (not yet explained) exception to this trend is for Cu target in ps ablation regime. The plasma heating by the ns pulses leads again to higher temperatures compared to the ps and and fs regimes, although for the heaviest atoms (Cu and Zn) this trend is reversed. Our results are in good agreement with previous studies which focused on differences observed in the excitation temperature [35,36] for plasmas generated in various ablation regimes. We note that the evolution of the excitation temperature with the atomic mass (presented in Figure 3b) does not depend significantly on the measuring distance, as the same dependence was observed at 1 mm and 20 mm from the target. A significant decrease (~50%) of the excitation temperature is observed over the first 5 mm from the target. We must note however that at longer distances the

excitation temperature calculation can be strongly affected by errors due to the decrease of the signal/noise ratio and possible (expected) deviations from the LTE, related to the electron density decrease and the transition of the LPP towards a predominant collisionless expansion regime.

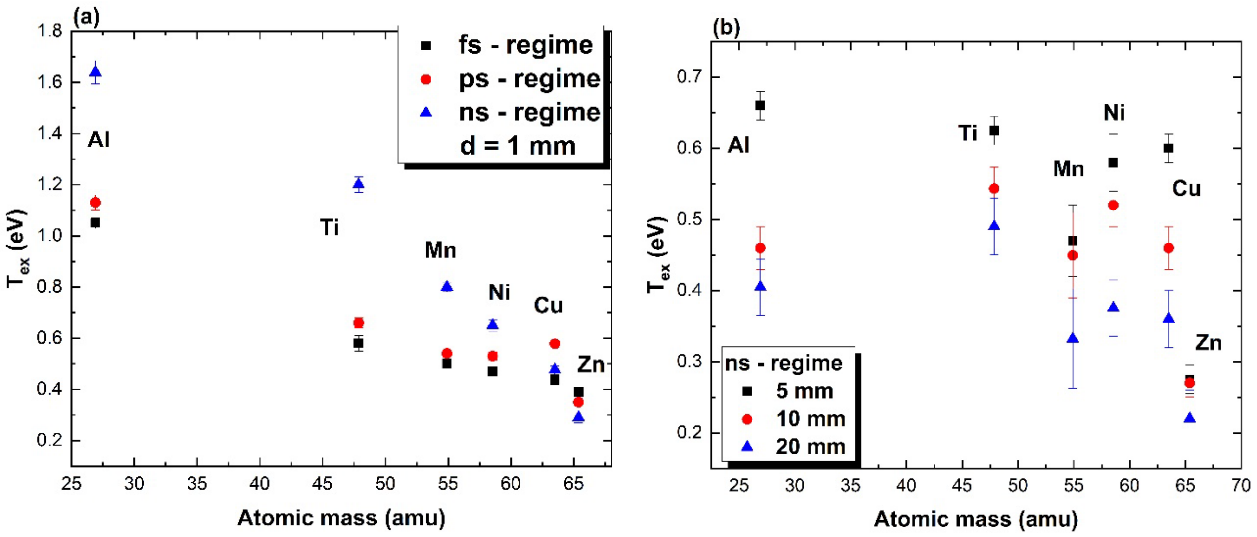

Figure 3. Excitation temperatures vs target material atomic mass at (a) 1mm and (b) 5mm, 10 mm, 20 mm from the target.

When investigating the impact of the heat of vaporization or that of the melting point of the metallic targets on the excitation temperature of the ejected atoms, we observe a similar dependence as in the previous case of expansion velocity (Figure 2b, c), *i.e.* the excitation temperature increases as the heat of vaporization and the melting point increase. These results are in good agreement with our previous interpretation on the effect of the properties like vaporization heat or melting point, where we saw an increase of the kinetic energy of the particle. With this augmentation the probability of multiple collisions increases and thus the possibility a higher T_{ex} induced by these collisions [45]. This result is better understood for fs and ps ablation regime, where the thermal effects are reduced, while the electron-ion energy transfer (in the bulk material) and the electron heat conduction times are significantly higher than the pulse time-width.

In order to build a stronger image of these dependences, we also looked at other parameters (electrical/thermal conductivity, boiling point, ionization potential), but no clear connection with the excitation temperature was found, just a general decreasing trend. For example, the Mn and Cu plasmas have similar excitation temperatures, despite the large differences between their thermal or electrical conductivities. The plasma with the second highest value of the excitation temperature was the one generated on a Ti target, the material with the highest heat of vaporization, boiling point and ionization energy, while the lowest value was found for the plasma generated on the material having the lowest heat of vaporization, melting point and ionization energy (Mn).

Comparison between the three ablation regimes can be rather difficult, especially if we take a broader look at all ablation mechanisms involved. In the case of nanosecond laser irradiation, the ablation process is dominated by thermal processes which lead to melting and vaporization, material removal and the absorption of the incident pulse energy by the plasma. By contrast, for shorter ablation regimes (fs and ps laser ablation) the laser pulse is shorter than the characteristic relaxation times [6]. The heat load to the surrounding material is reduced, allowing a well-defined heat-affected area in contrast to ns regime where the re-solidification of melted layers leads to irregularities on the material surface [6,42]. For low fluence fs-laser irradiation, the Coulomb explosion is the dominant ejection mechanism, while at sufficiently high laser intensities the phase explosion is followed by non-thermal vaporization of the bulk material and becomes the main mechanism for material removal [6]. Therefore, alternative plasma diagnostics, which can offer more localized spatio-temporal information, are necessary.

3.3 Langmuir probe measurements

The diagnostic chosen as an alternative for OES measurements was the Langmuir Probe (LP) method in its time-resolved sequential approach. In the framework of the LP technique, all plasma parameters that are derived are only related to the charged particles (electron temperature, density, ionic temperature, thermal velocity, plasma potential). Although the thermal velocity describes mainly the movement of the electrons, it is related to the local thermal energy of the whole plume. In a similar manner, the drift velocity determined using the method presented in [31] can be related to the overall kinetic energy of the ions. The energy of the ejected particles, according to [41,42], can be correlated to some extent to the cohesive energy of the lattice ions, therefore we will first look at the dependences on the material properties related to the electrostatic ablation mechanism.

Increased thermal and drift velocities were observed (Figure 4 a,b) for LPPs generated on targets with high electrical conductivity. According to a theoretical study of Bulgakova et al. [6], when Coulomb Explosion (CE) is considered as (the main) particle removal mechanism, a highly conductive material irradiated above the threshold fluence may lead to the ejection of a high density of electrons. This is followed by the formation of an intense positive charge region on the target surface in the early moments of the laser ablation process. The charge separation leads to a strong ambipolar electric field which acts as a driving force for the kinetics of the ejected ions.

Our results show a quasi-linear increase for the thermal velocity from values of 2 km/s for the material with the lowest electrical conductivity (Mn) to ≈ 5 km/s for Cu which has the highest electrical and thermal conductivities (Figure 4a). The highest thermal velocities are seen for the ps LPP. Although the increasing trend can be observed at all investigated ablation regimes, some discrepancies between different regimes can be understood as a direct result of the higher lateral expansion in the nanosecond regime coupled with high localization of the LP technique.

The drift velocities present a steep rise for low conductivity elements reaching a quasi-saturation regime after $(20 - 40) \times 10^6$ Sm^{-1}. Although the evolution with the electrical conductivity follows a similar trend for all the ablation regimes (ns, ps and fs), the highest values

are found for the nanosecond regime while the lowest ones are found for the fs regime (Figure 4b). These divergences from the results seen through ICCD fast camera imaging can be attributed to the high directionality of the fs and ps LPP compared to the ns one.

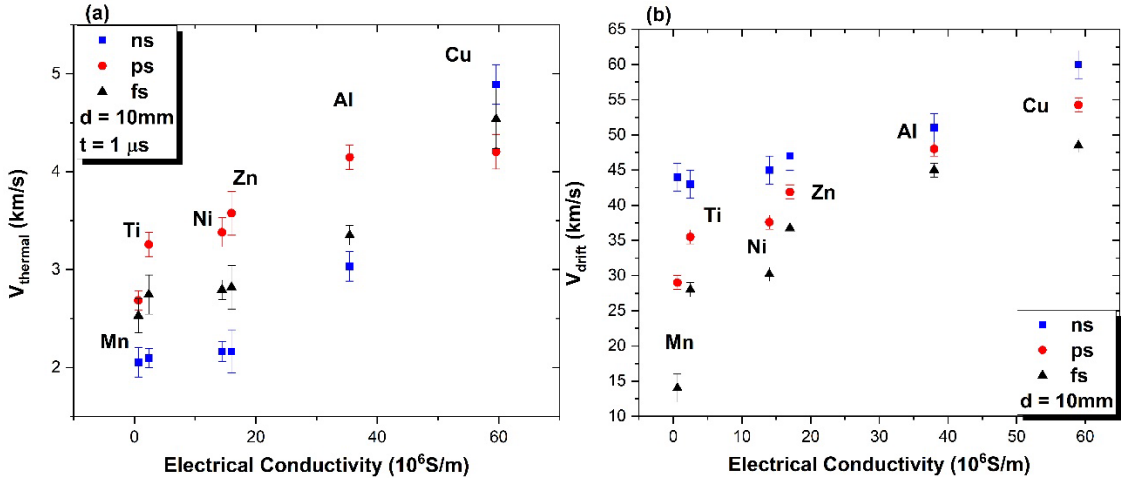

Figure 4. Electron thermal velocity (a) and ionic drift velocity (b) vs electrical conductivity of the target materials.

These results are also in good agreement with our previous findings [25], where the expansion velocities of LPP from multi-element chalcogenide targets increased as the electrical conductivity of the target was altered by the addition of Se_2Sb_3. We used a similar approach in [31] for fs-LPP on a wider range of metallic targets (Al, Ni, Mn, Cu, In, Te, W) and we have found the same quasi-linear increase. There we reported an exception to this rule for the Te plasma explained by the low boiling point (≈ 1261 K) compared to all other investigated materials which let us on the role of thermal mechanisms in this plasma generation.

In Figure 5 we have represented the evolution of the plasma potential and electronic temperature with the electrical conductivity of the metals. We choose to focus more on the electronic temperature (T_e) instead of the ionic (T_i) one, as T_e represents a well-defined "local" (in space and time) measurement, and has a better theoretical understanding in the framework of the Langmuir Probe method. We note however that T_i is following roughly the same evolution as the electron temperature. Both quantities were derived at a certain distance away from the target, from time-resolved LP characteristics of current-voltage (*I-V*) type [31]. The plasma potential and the electronic temperature present a steep increase for low conductivity elements reaching a quasi-saturation regime after 20×10^6 Sm^{-1}. The same dependence was reported by our group [31] for a different set of materials (Al, Ni, Mn, Cu, In, Te, W). We would like to note that although some materials are different, the range of conductivities is the same, as both studies contain Cu which has the highest conductivity and Mn with the lowest value.

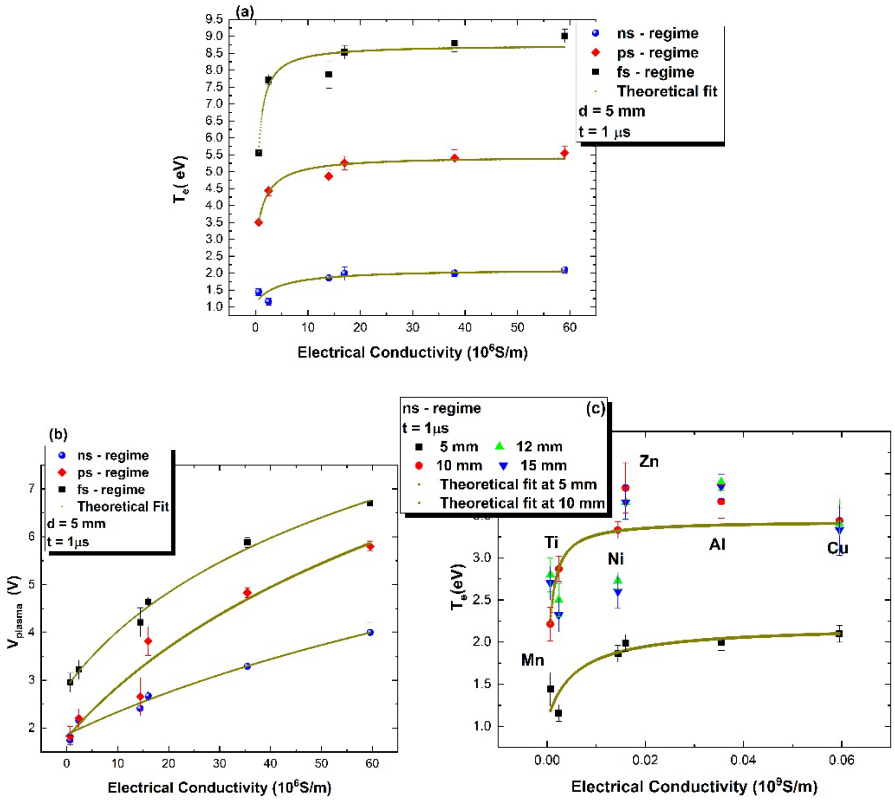

Figure 5. Electron temperature (a) and plasma potential (b) dependences on the electrical conductivity of the investigated metals fitted with the functions (1) and (2), respectively, and electron temperature dependence (c) on the electrical conductivity for 1 μs delay, at different target-probe distances for the ns-LPP

The relationship between the electronic temperature and the electrical conductivity of the materials can be explained by admitting a contribution from Coulomb Explosion (CE) mechanism [6] to the overall particle ejection and expansion in all ablation regimes. This will automatically give a relation of proportionally between the charge carrier mobility and the electric current density generated by laser irradiation, which can be exploited through the LP method. Within the "classical" LP method, parameters like T_e are extracted by fitting the linear increase of the electronic region in a logarithmic representation of the *I-V* characteristic [31]. Since the electrical conductivity (σ) is proportional to the charge mobility and subsequently to the collected probe signal, we proposed in [31], in the fs ablation regime, a $1/\sigma$ dependence for T_e, in the form:

$$T_e(\sigma) = c_T - \frac{b_T}{\sigma + a_T} \tag{1}$$

where a_T (Sm^{-1}), b_T ($eV.Sm^{-1}$), and c_T (eV) are fitting parameters. This dependence is also confirmed here, both for the ps and ns regimes (see Figure 5a), meaning that the fingerprint of electrostatic ablation mechanisms remains noticeable even though the thermal ablation mechanisms become more prominent.

We applied the same formalism to the plasma potential, which was determined from the logarithmic representation of the electronic current *vs.* the probe voltage, as the inflection point. The universality of the empirical logarithm-type function proposed in [31]:

$$V_{Plasma}(\sigma) = a_V + b_V \ln(c_V + \sigma) \quad (2)$$

where a_V (V), b_V (V), and c_V (Sm^{-1}), are fitting parameters, to explain the relationship between the plasma potential and the target electrical conductivity in fs ablation, is now confirmed (see Figure 5b) as the it can be used to also describe the data for ps- and ns-generated plasmas.

After the fitting for each ablation regime, a set of characteristic parameters were extracted characterizing the data collected at 5 mm from the target after 1 μs, and they are presented in Table 1. We observe some difference among the values for each ablation regime. All parameters determined for fs LPP are higher than those for ps or ns. At this moment it is difficult to assess if the evolution of the fitting parameters can be directly related to the weighted contribution of the Coulomb explosion as the main ablation mechanism. A subsequent study regarding the variation of these plasma parameters with other metal characteristics (such as atomic weight or ionization potential) did not reveal any direct correlation, and thus a clear physical description of these empirical fitting parameters was not possible. However, we can state that the proposed empirical functions describe well the considered set of materials in the range for the laser fluence / background pressure conditions used in this study.

Table 1. The values of the empirical parameters for each ablation regime derived after fitting with Eqs. (1) and (2) the excitation temperature and the plasma potential evolution with the electrical conductivity of the metallic targets.

Parameter	**Femtosecond regime**	**Picosecond regime**	**Nanosecond regime**
a_T ($S\,m^{-1}$)	0.00914(1)	0.00497(3)	0.00341(2)
b_T ($eV.S\,m^{-1}$)	0.358(2)	0.0115(6)	0.0038(4)
c_T (eV)	9.12(3)	3.221(5)	2.13(8)
a_V (V)	14.75(6)	13.1(1)	10.6 (5)
b_V (V)	4.7(2)	3.72(5)	3.16 (4)
c_V ($S\,m^{-1}$)	0.061(2)	0.03(1)	0.0183(7)

We would like to emphasize that the "universal" trends revealed by Eqs. (1) and (2) cover a wide range of target conductivity values (approximately two orders of magnitude), and a wide range of electron temperature values (0.2 - 9 eV) and plasma potentials (1– 7 V). To our knowledge this is the first report of a mathematical correlation between the plasma plume parameters and the

target material properties in all ns, ps and fs ablations regimes, and it stands as the main finding of this report. However, we must stress that the empirical parameters derived in Table 1 are specific to a particular plasma volume investigated at a specific moment of time, thus a systematic mapping of the plasma space-time evolution is needed for a complete description. We represented in Figure 5c the ns-LPP electronic temperature dependence on the electrical conductivity at different distances from the target. The result revealed similar dependence between T_e and the electrical conductivity although the data becomes more scattered for distances above 5 mm. For longer distances, the data are significantly scattered and we can speculate on a "*loss of memory*" for the plasma with respect to the initial stages of expansion.

Because our experiments were performed on a wide range of elements and in three different ablation regimes, the comparison with other similar attempts are necessary in order to confirm our newly proposed dependences and the generalization of other data existent in literature. This is not a simple task as the main parameter considered in literature is the total ionic density and it is usually compared with the bonding energy of the ions in the crystalline lattice [39,41,42,46]. The dependences proposed in [41,42] are focused on the volatility of the materials, which can be also described by the heat of vaporization or the melting point. Let us consider for example Figure 6, where we represented the saturation ion density (recorded at 10 μs delay) as a function of the melting point of the target material, function described by a decreasing trend. A similar observation was found in [42] where the ns ablation plasmas of different targets (Mo, Fe, Mn, Cu, Al, Zn, Pb and Sn) were investigated. A significant decrease in the ablation efficiency (estimated as a function of the ablated crater depth) with the increase of the melting point was observed. The same type of influence of the melting point on the ablation yield was found by Thestrup et al. [41] when investigating the ns-laser produced plasmas of metallic targets (Al, Cu, Zn, Bi and Ag). A decrease of about two orders of magnitude in ablation yield with the increase of cohesive energy was observed by Schou et al. [41]. In [41] both melting point and cohesive energy are considered as a measure of the degree of volatility. Our present results act as a generalization of the previous results, as we find a decrease in the ionic density with the increase of the melting point in all three ablation regimes. Higher ionic densities were found for the ns and ps regime as opposed to the fs one due to the increasing contribution of secondary (thermal) ablation mechanism to particle ejection. This result can be now coupled with the dependences seen for the drift velocity of excitation temperature with the vaporization heat of the target. The increase in the vaporization heat (bonding energy) does lead to an overall decrease in ionic density although the overall kinetic energy of the ejected particles is increasing.

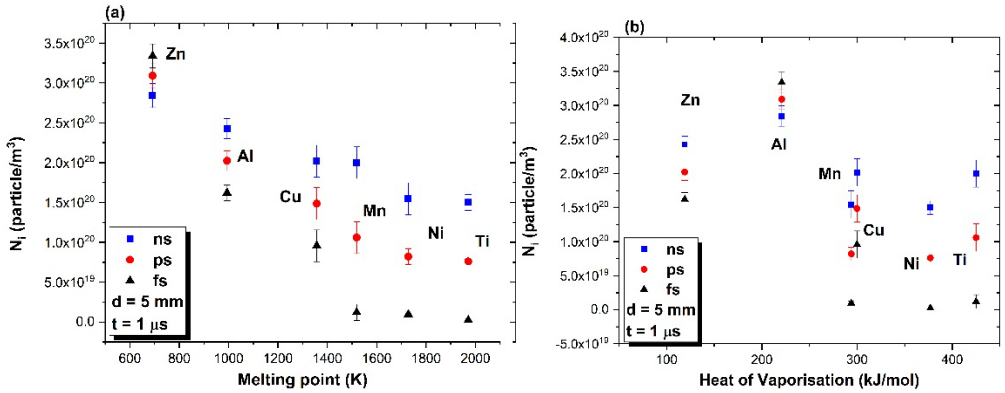

Figure 6. Ionic density dependence on the melting point (a) and the heat of vaporization (b) of the target materials.

4. Conclusions

We report here on a series of relationships between the physical properties of the ablation target and the kinetic and energetic parameters of the laser-produced plasma plumes, characterizing three different irradiation regimes (ns, ps and fs). The experimental approach involves the use of ICCD fast camera imaging, optical emission spectroscopy and Langmuir probe method implemented for the study of plasma generated on ablation on various single-element metallic targets (Al, Ti, Mn, Ni, Cu, Zn) The experimental data revealed fundamental differences between plasma generated in each ablation regime which are attributed to specific mechanisms involved in material removal. The optical investigation revealed a good correlation between the excitation temperature or expansion velocities and the atomic mass, result explained on the basis of a thermal ejection mechanism. A general relation validated in all three ablation regimes was found between the electrical conductivity of the materials and the expansion velocity, electron and ion temperature and plasma potential. These relationships are discussed in the framework of the Coulomb explosion scenario and come as generalizations of our previous reported results. Some results have been well correlated with the formation mechanisms of the two-plasma structure, but it is difficult specify if there is no other contribution to these evolutions. All the discussion regarding the energetic plasma parameters like electronic/excitation temperatures, plasma potential, thermal/drift velocities and how the ablation mechanisms are influencing the dynamics of the ejected particles was made on the basis that our empirical relationship transcends all three ablation regimes. this lead to the confirmation and generalization of the already known ion density- vaporization heat relationship. The strength of the proposed relations can be further tested against different types of materials (dielectrics, semi-conductors, etc.) and other experimental conditions in terms of background pressure or laser fluence.

References

[1] R.W. Eason (Ed.), Pulsed Laser Deposition of Thin Films: Applications-Led Growth of Functional Materials (John Wiley, New Jersey, 2006).

[2] D.B. Chrisey, G. K. Hubler (Eds.), Pulsed Laser Deposition of Thin Films (John Wiley, New Jersey, 1994).

[3] K. Sugioka, M. Meunier, A. Piqué (Eds.), Laser Precision Microfabrication (Springer, Berlin, Heidelberg, 2010).

[4] S.C. Singh, H.B. Zeng, C. Guo, W. Cai (Eds.), Nanomaterials: Processing and Characterization with Lasers (Wiley-VCH, Weinheim, 2012).

[5] R. E. Russo, X. Mao, J. J. Gonzales, V. Zorba, J. Yoo, Laser Ablation in Analytical Chemistry, Anal. Chem. 85 (2013) 6162-6177.

[6] N.M. Bulgakova, R. Stoian, A. Rosenfeld, I.V. Hertel, W. Marine, E.E.B. Campbell, A general continuum approach to describe fast electronic transport in pulsed laser irradiated materials: The problem of Coulomb explosion, Appl. Phys. A 81 (2005) 345–356.

[7] D.B. Geohegan, Fast ICCD-Photography of YBCO Laser Ablation Plume Propagation in Vacuum and Ambient Oxygen, Appl. Phys. Lett. 60 (1992) 2732–2734.

[8] A. Aliverdiev, D. Batani, R. Dezulian, T. Vinci, A. Benuzzi-Mounaix, M. Koenig, V. Malka, Hydrodynamics of laser-produced plasma corona measured by optical interferometry, Plasma Phys. Control. Fusion 50 (2008) 105013.

[9] M. Feinaeugle, A.P. Alloncle, P. Delaporte, C. Sones C., R.W. Eason, Time-resolved shadowgraph imaging of femtosecond laser-induced forward transfer of solid materials, App. Surf. Sci. 258 (2012) 8475–8483.

[10] S.S. Harilal, B.E. Brumfield, N.L. LaHaye, K.C. Hartig, M.C. Phillips, Optical spectroscopy of laser-produced plasmas for standoff isotopic analysis, Appl. Phys. Rev. 5 (2018) 021301.

[11] A.D. Sappey, T.K. Gamble, Laser-fluorescence diagnostics for condensation in laser-ablated copper plasmas, Appl. Phys. B 53 (1991) 353–361.

[12] A. Mendys, M. Kański, A. Farah-Sougueh, S. Pellerin, B. Pokrzywka, K. Dzierżęga, Investigation of the local thermodynamic equilibrium of laser-induced aluminum plasma by Thomson scattering technique, Spectrochim. Acta B 96 (2014) 61-68.

[13] J. Chen, T. Lippert, A. Ojeda-G-P, D. Stender, C.W. Schneider, A. Wokaun, Langmuir probe measurements and mass spectrometry of plasma plumes generated by laser ablation of $La_{0.4}Ca_{0.6}MnO_3$, J. Appl. Phys. 116 (2014) 73303.

[14] C. Ursu, P. Nica, Diagnosis of carbon laser produced plasma by using an electrostatic energy analyzer, J. Optoelectron. Adv. Mater. 15 (2013) 42–45.

[15] T. Donnelly, J.G. Lunney, S. Amoruso, R. Bruzzese, X. Wang, X. Ni, Dynamics of the plumes produced by ultrafast laser ablation of metals, J. Appl. Phys. 108 (2010) 043309.

[16] D. Doria, A. Lorusso, F. Belloni, V. Nassisi, Characterization of a nonequilibrium XeCl laser-plasma by a movable Faraday cup, *Rev. Sci. Instrum. 75* (2004) 387-392.

[17] A. Ojeda-G-P, M. Döbeli, T. Lippert, Influence of Plume Properties on Thin Film Composition in Pulsed Laser Deposition, Adv. Mater. Interfaces 5 (2018) 1701062.

[18] J. Schou, M. Gansukh, R.B. Ettlinger, A. Cazzaniga, M. Grossberg, M. Kauk-Kuusik, S. Canulescu, Pulsed laser deposition of chalcogenide sulfides from multi- and single-component targets: the non-stoichiometric material transfer, Appl. Phys. A 124 (2018) 78.

[19] S. Canulescu, M. Döbeli, X. Yao, T. Lippert, S. Amoruso, J. Schou, Nonstoichiometric transfer during laser ablation of metal alloys, Phys. Rev. Mater. 1 (2017) 073402.

[20] C. Focsa, S. Gurlui, P. Nica, M. Agop, M. Ziskind, Plume splitting and oscillatory behavior in transient plasmas generated by high-fluence laser ablation in vacuum, Appl. Surf. Sci. 424 (2017) 299-309.

[21] A. Ojeda-G-P, C.W. Schneider, M. Döbeli, T. Lippert, A. Wokaun, Plasma plume dynamics, rebound, and recoating of the ablation target in pulsed laser deposition, J. Appl. Phys. 121 (2017) 135306.

[22] G. Baraldi, A. Perea, C.N. Afonso, Dynamics of ions produced by laser ablation of several metals at 193 nm, J. Appl. Phys. 109 (2011) 043302.

[23] T. Donnelly, J.G. Lunney, S. Amoruso, R. Bruzzese, X. Wang, C. Phipps, Plume dynamics in femtosecond laser ablation of metals, 643 (2010) 643–655.

[24] K.K. Anoop, M.P. Polek, R. Bruzzese, S. Amoruso, S.S. Harilal, Multidiagnostic analysis of ion dynamics in ultrafast laser ablation of metals over a large fluence range, J. Appl. Phys. 117 (2015) 083108.

[25] S. Irimiciuc, R. Boidin, G. Bulai, S. Gurlui, P. Nemec, V. Nazabal, C. Focsa, Laser ablation of $(GeSe2)_{100-x}(Sb_2Se_3)_x$ chalcogenide glasses: Influence of the target composition on the plasma plume dynamics, Appl. Surf. Sci. 418 (2017) 594–600.

[26] C. Focsa, P. Nemec, M. Ziskind, C. Ursu, S. Gurlui, V. Nazabal, Laser ablation of $AsxSe_{100-x}$ chalcogenide glasses: Plume investigations, Appl. Surf. Sci., 255, 5307 (2009)

[27] A.F Semerok, B. Salle, J.L. Lacour, J.F. Wagner, G. Petite, O. Gobert, P. Meynadier, M. Pedrix, Femtosecond, Picosecond and Nanosecond Laser Microablation: Laser Plasma and Crater Investigation, Proc. SPIE 4424 (2001) 574–579.

[28] G. Pompilian, S. Gurlui, P. Nemec, V. Nazabal, M. Ziskind, C. Focsa, Plasma Diagnostics in Pulsed Laser Deposition of GaLaS Chalcogenides, Appl. Surf. Sci. 278 (2013) 352-356.

[29] G. Bulai, O. Pompilian, S. Gurlui, P. Nemec, V. Nazabal, N. Cimpoesu, B. Chazallon, C. Focsa, Ge-Sb-Te Chalcogenide Thin Films Deposited by Nanosecond, Picosecond, and Femtosecond Laser Ablation, Nanomaterials 9 (2019) 676

[30] G. Dascalu, G. Pompilian, B. Chazallon, O. Caltun, S. Gurlui, C. Focsa, Femtosecond Pulsed Laser Deposition of Cobalt Ferrite Thin Films, Appl. Surf. Sci. 278 (2013) 38-42.

[31] S.A. Irimiciuc, S. Gurlui, G. Bulai, P. Nica, M. Agop, C. Focsa, Langmuir probe investigation of transient plasmas generated by femtosecond laser ablation of several metals: Influence of the target physical properties on the plume dynamics, Appl. Surf. Sci. 417 (2017) 108–118.

[32] P. Nica, S. Gurlui, M. Osiac, M. Agop, M. Ziskind, C. Focsa, Investigation of femtosecond laser-produced plasma from various metallic targets using the Langmuir probe characteristic, Phys. Plasmas 24 (2017) 103119.

[33] P. Nica, S. Gurlui, M. Agop, C. Focsa, Oscillatory regimes of Langmuir probe current in femtosecond laser-produced plasmas: Experimental and theoretical investigations, Appl. Surf. Sci, 481 (2019) 125-132

[34] S.A. Irimiciuc, S .Gurlui, P. Nica, C. Focsa, M. Agop, A compact non-differential approach for modeling laser ablation plasma dynamics, J. Appl. Phys. 121 (2017) 083301

[35] J.R. Freeman, S.S. Harilal, P.K. Diwakar, B. Verhoff, A. Hassanein, Comparison of optical emission from nanosecond and femtosecond laser produced plasma in atmosphere and vacuum conditions, Spectrochim. Acta B 87 (2013) 43–50.

[36] B. Verhoff, S.S. Harilal, J.R. Freeman, P.K. Diwakar, A. Hassanein, Dynamics of femto- and nanosecond laser ablation plumes investigated using optical emission spectroscopy, J. Appl. Phys. 112 (2012) 093303.

[37] C. Ursu, O.G. Pompilian, S. Gurlui, P. Nica, M. Agop, M. Dudeck, C. Focsa, "Al_2O_3 ceramics under high-fluence irradiation: plasma plume dynamics through space- and time-resolved optical emission spectroscopy", Appl. Phys. A **101** (2010) 153-159..

[38] A.V. Bulgakov, N.M. Bulgakova, Thermal model of pulsed laser ablation under the conditions of formation and heating of a radiation-absorbing plasma, Quantum Electron. 29 (2007) 433–437.

[39] V. Schmidt, W. Husinsky, G. Betz, Dynamics of laser desorption and ablation of metals at the threshold on

the femtosecond time scale, Phys. Rev. Lett. 85 (2000) 3516–3519.

[40] S. Amoruso, X. Wang, C. Altucci, C. De Lisio, M. Armenante, R. Bruzzese, Thermal and nonthermal ion emission during high-fluence femtosecond laser ablation of metallic targets, 77 (2000) 3728–3730.

[41] B. Thestrup, B. Toftmann, J. Schou, B. Doggett, J.G. Lunney, Ion dynamics in laser ablation plumes from selected metals at 355 nm, Appl. Surf. Sci. 197–198 (2002) 175–180.

[42] B. Salle, C. Chaleard, V. Detalle, J.-L. Lacour, P. Mauchien, C. Nouvellon, A. Semerok, Laser ablation efficiency of metal samples with UV laser nanosecond pulses, Appl. Surf. Sci. 138–139 (1999) 302–305.

[43] N. M. Bulgakova, A. Bulgakov, O. F. Bobrenok, Double layer effects in laser-ablation plasma plumes, Phys. Rev. E 62 (2000) 5624-5635.

[44] S. Gurlui, M. Sanduloviciu, M. Strat, G. Strat, C. Mihesan, M. Ziskind, C. Focsa, "Dynamic space charge structures in high fluence laser ablation plumes", J. Optoelectron. Adv. Mater. 8 (2006) 148-151.

[45] R.K. Singh, A. Kumar, B.G. Patel, K.P. Subramanian, Role of ambient gas and laser fluence in governing the dynamics of the plasma plumes produced by laser blow off of LiF–C thin film, J. Appl. Phys. 101 (2007) 103301.

[46] K.H. Leitz, B. Redlingsher, Y. Reg, A. Otto, M. Schmidt, Metal ablation with short and ultrashort laser pulses, Phys. Procedia. 12 (2011) 230–238.